



# Advanced *in vivo* fluorescence microscopy of neural electronic interface

Qianru Yang and X. Tracy Cui\* 

Neuroelectronic devices are essential tools in neuroscience research, diagnosis, and/or treatment of neurological diseases, as well as in neuro-prosthetics and brain–computer interfaces. Despite a long history of application, neuroelectronic devices are still facing challenges of unsatisfactory chronic stability and a lack of understanding of cellular mechanisms for recording and stimulation. To improve the information transfer between the neural tissue and electronic devices, a comprehensive understanding of the biological activities around the neural electrode is critical. *In vivo* fluorescent microscopy technologies are rapidly developing and have revolutionized our understanding of cellular dynamics in response to neural interfacing materials. Here, we will provide an overview of the *in vivo* fluorescence microscopy systems and imaging configurations for studying the neural electronic interface, as well as recent findings in biological mechanisms learned using these advanced optical imaging modalities. Finally, we will discuss the current challenges and future directions.

## Introduction

Since the discovery of action potentials, neural electrodes have been vital tools to read out and modulate neural activities. By recording and stimulating with implanted electrodes, researchers can determine the functions and connections of different brain regions.<sup>1,2</sup> The clinical value of brain electrodes was found first in treating tremor with deep brain stimulation (DBS), followed by successful treatments of a variety of neurological diseases, such as depression, epilepsy, pain, addiction, dementia, and stroke recovery.<sup>3</sup> Neural prosthetics based on implanted neural electrodes are evolving at a rapid pace and have shown great potential in restoring functions of the central nervous system (CNS), including motor, visual, auditory, somatosensory sensation, etc.<sup>4–6</sup> Despite these progresses, the mechanisms of neural prosthetics at the cellular level and the interactions between the implanted device and host tissue remain poorly understood, and the elucidation of such is absolutely important for improving their efficiency, precision, naturalness, and safety.

To date, all of the neural interfacing implants are still facing a significant challenge—the foreign body responses of brain tissue, including blood–brain barrier (BBB) disruption, microglia activation, macrophage infiltration, astrogliosis, fibrosis,

and neuronal loss and neurodegeneration.<sup>7</sup> These responses are believed to contribute to the low yield and degradation of neural recording. Traditionally, postmortem histochemistry has been the gold standard to evaluate biological responses toward neural implants because of the rich choices of chemical compounds and antibodies that can label many types of biomolecules and cells. However, postmortem histochemistry only provides a snapshot at discrete end points, omitting the dynamic information in between. Additionally, conventional histochemistry requires removal of the implant for tissue slicing and staining, which inevitably damages the original tissue–device interface. Device-capture histology maintains the electrode–tissue interface by slicing the tissue parallel to the probe shank in thick sections (350–450  $\mu\text{m}$ ).<sup>8</sup> This method allows direct visualization of the probe *in situ*, but is still a postmortem approach.

Recent technology advancements in *in vivo* fluorescence microscopy allow investigations of real-time and long-term changes of cellular activity in living animals. Here, we will discuss the currently available *in vivo* fluorescence microscopy technologies for studying cellular activities around implanted neural electronics and findings obtained using these imaging technologies.

Qianru Yang, University of Pittsburgh Swanson School of Engineering, Pittsburgh, USA; qiy24@pitt.edu  
X. Tracy Cui, University of Pittsburgh Swanson School of Engineering, Pittsburgh, USA; xic11@pitt.edu  
doi:10.1557/s43577-023-00530-7

### In vivo fluorescence microscopy

*In vivo* fluorescent imaging is a well-established and widely used method to study biological systems. There are three most popular types of *in vivo* fluorescence imaging methods: wide field microscopy, confocal microscopy, and multiphoton microscopy. Wide field microscopy illuminates a large field (typically enough to cover the whole cranial window on rodents) and collects emission light by a camera on a fluorescence microscope.<sup>9</sup> It is relatively low cost and has faster imaging speed compared to confocal and multiphoton microscopy, but lacks depth specificity because it receives emitted light from both in-focus and out-of-focus planes, making it difficult to visualize fine cellular structures in thick tissues.<sup>10</sup> Technological improvements for high-resolution wide field microscopy are growing.<sup>11</sup> For instance, structured illumination and reconstruction algorithms can remove out-of-focus signals, and when combined with adaptive optics, have achieved synapse-resolving imaging *in vivo*.<sup>10,12</sup>

Confocal microscopy reduces the out-of-focus signals by focusing the illumination light to the focal point and placing a pinhole before the detector, enabling optical sectioning of thick tissue.<sup>13</sup> However, due to scattering and absorption of light in the biological tissue, the imaging depth is limited. One approach to increase imaging depth is to extend the excitation and emission wavelengths to 1000–1700 nm, the second near-infrared window (NIR-II).<sup>14</sup> Together with development of long wavelength fluorescent probes and improvement of single-photon detectors, the imaging depth of confocal microscopy has recently demonstrated up to 1.7 mm below the surface of the mouse brain.<sup>15,16</sup>

Multiphoton laser scan microscopy has been the most widely employed high-resolution *in vivo* fluorescent imaging method. Multiphoton microscopy utilizes a laser with a doubled or tripled long wavelength compared to single-photon fluorescent microscopy. The fluorescence excitation requires two or more photons to arrive at the point simultaneously, which significantly reduces the out-of-focus fluorescence excitation therefore decreases out-of-focal plane noises and is safer for long-term imaging than traditional single-photon microscopy. In addition, the longer laser wavelength can penetrate deeper into the scattering tissue. Two-photon

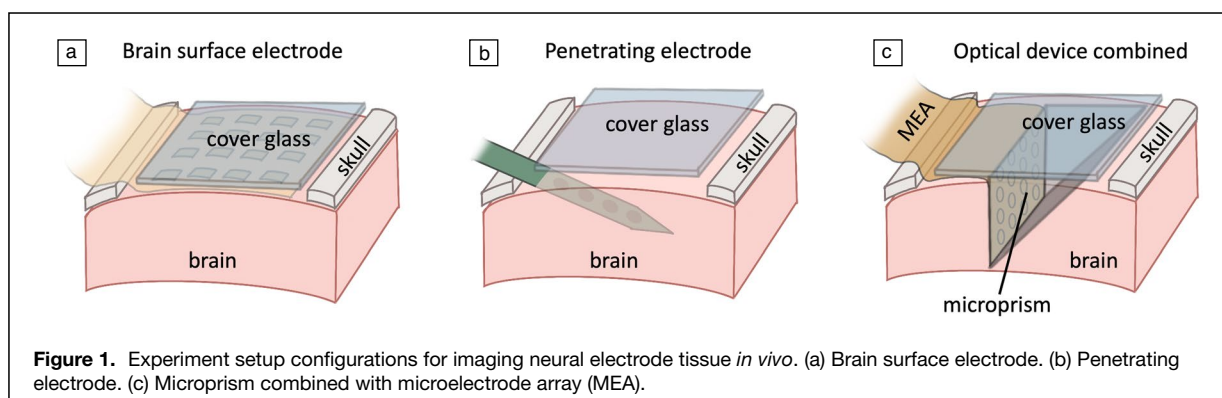
microscopy typically can reach 500- $\mu\text{m}$  deep, and three-photon microscopy about 900- $\mu\text{m}$  deep, and using longer wavelength could further improve the imaging depth to  $\sim 1.6$  mm.<sup>17,18</sup> Despite the high resolution and deep optical penetration, the imaging speed and the field of view of traditional multiphoton microscopy is limited to  $<10$  Hz and  $<1$  mm<sup>2</sup>.<sup>19</sup> Methodology advancements of multiphoton microscopy are heading toward large field of view, kilohertz scan rate, multiplane, multiregion, and miniaturization for imaging in free-behaving animals.<sup>20–23</sup>

### In vivo imaging configurations for electrode-tissue interface studies

Currently, there are three major types of setup configurations for visualizing brain tissue and neural electronic device interfaces with optical imaging systems differentiated based on the position of the electrode and optical light path (**Figure 1**).

#### Brain surface electrodes

Advancements in fabricating transparent electrode arrays have allowed optical imaging directly through a brain surface electrode. After craniotomy, the electrodes can be positioned above or underneath the dura to record the electrocorticogram (ECoG) signals and to deliver electrical stimulation (**Figure 1a**). The electrodes are usually flexible, sheet-like, and consist of several layers of different materials. Typically, the conductive material is sandwiched between insulation layers, except for the electrode sites and the bonding pads. The insulation materials need to be nonconductive, flexible, transparent, and biocompatible. Popular polymers for the insulation substrate are poly(dimethylsiloxane) (PDMS), parylene C, parylene HT, SU-8, polyimide, liquid crystal polymer, hydrogel,<sup>24</sup> etc. Different materials have different properties and different ways of fabrication that could influence their applications.<sup>25</sup> The commonly used conductive materials include metals, carbon/graphene,<sup>26,27</sup> indium tin oxide (ITO),<sup>28</sup> and poly(3,4-ethylenedioxythiophene) (PEDOT)-based conducting polymers. Metallic materials, such as platinum (Pt), gold (Au), and iridium/iridium oxide (Ir/IrOx), have a long history of making neural electrodes due to their high conductivity, chemical inertness, high charge-storage capacity, and good biocompatibility. However, metallic materials are not transparent. The



accessible region for optical imaging is often limited to areas outside of metal parts. To improve the light transmittance of metal parts, several groups have developed different methods to create mesh-shaped metal.<sup>29–31</sup> There are also an increasing number of studies of other materials with better optical transparency. For example, the carbon-nanotube/PDMS electrode array has a greater than 85% transmittance across light wavelengths from 400 to 2500 nm.<sup>32</sup> However, the electrochemical impedance of most of the transparent materials is high. Surface modification with conductive polymers or nano-sized metal have been used to improve the electrochemical impedance of transparent materials at the cost of decreased transparency.<sup>26,27</sup>

Multiphoton imaging and concurrent electrophysiological recording/stimulation through transparent ECoG arrays have been demonstrated in animals.<sup>33</sup> The animals are either transgenically labeled with fluorescent proteins or locally injected with virus or dyes to indicate neural activity. One big challenge for concurrent multiphoton imaging and electrophysiology recording is the photoelectric artifact. The photoelectric effect happens when the light hits the electrode material (sites and traces), electrons in the material absorb the energy and are emitted, producing a current that can be captured by the recording equipment.<sup>34</sup> The amplitude of the artifact has been shown to be related with the laser power and scan rate.<sup>35,36</sup> This artifact is also stronger for metal materials because the electrons in metal have lower binding energy than nonmetal conductors.<sup>27,28,36</sup> Increasing transparency can effectively reduce the photoelectrical artifact. When the amplitude of the photoelectric artifact does not saturate the recording amplifier, it is possible to remove the recording artifact by post-processing algorithms, such as multiple band-stop filters or subtracting an average artifact template based on laser scanning triggers.<sup>35,37</sup>

Compared to intracortical microelectrodes, brain surface electrodes usually are limited to recording local field potentials (LFPs) and multiunit activity. Resolving single unit activities from surface electrodes is difficult because of the distance to neuronal somas. On the other hand, they are considered less invasive and introduce less damage to the underlying brain parenchyma tissue. Both epidural and subdural implants are usually encapsulated by collagenous tissue and inflammatory cells further increasing the distance to cortical neurons.<sup>38,39</sup> Softer implants that are more conformal to the brain curvature could reduce mechanical stress and fibrous encapsulation.<sup>40</sup> Yet, chronic *in vivo* imaging studies of brain surface electrode arrays have been rare.<sup>41</sup>

### Penetrating electrodes

To date, the most common imaging setup for studying foreign body responses and extracellular electrophysiology is to insert a silicon electrode device into the brain parenchyma at an angle between 30 and 45 degrees to the brain surface with electrode sites facing up<sup>42,43</sup> (Figure 1b). This allows the visualization of the electrode sites interfacing with the brain. Ultraflexible electrodes, developed for seamless integration in

the soft brain tissue, can also penetrate the brain, but usually need an accessory shuttle (a needle or a metal wire) or some temporary stiffening strategies to facilitate the insertion.<sup>44–46</sup> When the electrodes are transparent or sufficiently thin, they could be inserted more vertically without significantly affecting the imaging.<sup>45</sup>

In the acute setup, the cranial window can be left open for at least 6 h.<sup>47</sup> The advantage of having an open cranial window is to be able to rinse the blood out or make adjustment of the implant. However, with the skull open, the brain tissue is essentially exposed to pollution and pathogens in the environment that could influence the brain activity. Alternatively, the cranial window can be sealed with a cover glass and transparent filler such as saline, artificial cerebrospinal fluid (ACSF), silicone, agar, etc. Solid filler can also reduce the micromotion of the brain, thus improving the image stability.

In the chronic setup, the cranial window can be sealed with transparent medium and a cover glass on top. The clarity of the window, however, can be difficult to maintain.<sup>43</sup> For example, it was shown that the imageable depth drops from 600 to 300  $\mu\text{m}$  within a week.<sup>43</sup> The decreased window clarity and imaging depth resulted from cascades of host tissue responses including bleedings, bone regrowth, fibrous tissue thickening, recruitment of inflammatory cells at meninges and around the electrode, and sometimes infections due to contaminations or incomplete seal.<sup>48</sup> Placing the cover glass intimately onto the brain surface is the key to keeping a clear window by physically inhibiting tissue regrowth. Using a cover glass with a small hole and inserting silicon electrodes through the hole afterward, Mols et al. showed two-photon imaging of the electrode down to 500  $\mu\text{m}$  below the pia after two-week implantation and 200  $\mu\text{m}$  below the pia after 10-week implantation.<sup>49</sup> For flexible electrodes, it could be slightly easier to keep a clear window over time because the cover glass can be placed more seamlessly onto the brain surface.<sup>44,45</sup> Additionally, ultraflexible electrodes are expected to cast less chronic mechanical stress to the brain compared to stiff electrodes.

### Electrodes combined with penetrating optical devices

To date, *in vivo* imaging of surface and penetrating electrodes has been mostly limited to superficial layers (layer 1–3) of the cortex. In order to see deeper brain tissue, researchers have been developing optical devices that can break the imaging depth limit of conventional configurations. Optical fiber, microlens, and microprism are the three commonly used optical devices for deep brain imaging.

Optical fiber can be implanted to any depth into the brain and/or interface with other optical devices, allowing imaging in free-behaving animals due to its flexibility.<sup>50</sup> The same optic fiber can both deliver excitation light into the brain tissue and collect emission signals. The conventional optical fibers are based on silica, whereas other materials such as silk,<sup>51</sup> hydrogel, and synthetic polymers have also been investigated.<sup>52</sup> There are several categories of optic fiber, including conventional step-index fiber, fiber bundles, tapered optical

fiber, gradient refractive index (GRIN) fiber, etc.<sup>53,54</sup> The classic step-index fibers deliver light based on total internal reflection between the outer cladding and the inner core with distinct refractive indexes. Fiber bundles consist of up to ~100,000 densely packed step-index fibers to transform pixelated images.<sup>55</sup> The GRIN fiber has refractive index declines with radius from the central axis, so that light propagates at the same speed across different locations within the fiber. The tapered optical fiber has a special tapered tip compared to the traditional flat-cleaved tip, which can extend the light illumination and collection region from a restricted volume near the fiber tip to ~2 mm along the taper.<sup>56,57</sup> The size of optical fiber is customizable, ranging from ~10  $\mu\text{m}$  to several millimeters in diameter.<sup>58</sup> To enable electrophysiology, microwire electrodes (tetrodes) and flexible electrode arrays can be adhered to the side wall of the optic fibers.<sup>59</sup> Alternatively, multifunctional fibers have been fabricated by combining different components and materials for simultaneous electrophysiology and optical simulation/drug delivery.<sup>60</sup> However, optical fiber-based photometry has limitations on the spatial resolution as they measure integrated photon count from a large population of cells near the probe tip (within ~500  $\mu\text{m}$ ).<sup>61</sup>

Micro lenses, including miniaturized objective lenses and GRIN lenses, can provide better spatial resolution and signal efficiency than optic fibers. Objective lenses can provide the best resolution and fluorescent efficiency, but the miniaturization is challenging (minimally ~3 mm in diameter).<sup>62</sup> GRIN lenses can be miniaturized to 350–1000  $\mu\text{m}$  in diameter and can be customized to lengths from several millimeters to several centimeters to approach deep brain regions in rodents or larger animal models.<sup>63</sup> GRIN lenses can be used for wide field, confocal, multiphoton microscopy, or integrated with optic fibers.<sup>63–65</sup> Similar to optical fibers, stiff and flexible electrodes can be placed on the side wall of GRIN lenses.<sup>66</sup>

Microprisms are tiny glass prisms, with size customizable from 500  $\mu\text{m}$  to several millimeters. The coating (usually aluminum) on the slant side will reflect light at 90 degrees, changing the focal plane from horizontal to vertical. This vertical view is favorable for high resolution imaging of interlaminar activities.<sup>67</sup> Microprisms can be directly glued under the cover glass or combined with GRIN lens or optic fibers.<sup>68,69</sup> Flexible electrode arrays can be attached to the microprism imaging face after bending to comply the 90 degree angle formed between the microprism and the cover glass<sup>70</sup> (Figure 1c).

The footprint of optical devices is usually much larger than microelectrode arrays, as such tissue damages caused by implanting these optical devices bring about some concerns. Optic fibers or lenses smaller than 1 mm in diameter could be implanted without removing brain tissue but would squeeze or push tissue to the side or to the bottom, resulting in mechanical damage and chronic compression stress. Devices larger than 1 mm could require removing part of the brain tissue to reduce the compressive damage. During insertion, the optical devices will inevitably damage some blood vessels, and the bleeding will cast a shadow in the images due to light

absorption by red blood cells. It has been reported that bleeding and vascular remodeling take about two weeks to settle down after the 1-mm-microprism implantation,<sup>71</sup> while the microglial responses need four to eight weeks to return to the homeostatic state.<sup>72</sup> In addition, because most optical devices are rigid and need to be anchored to the skull, the mechanical mismatch between the brain tissue and the optical glasses increases the possibility of postsurgery damage due to micro-motion.<sup>73</sup> Soft optical fibers have shown reduced inflammatory responses compared to rigid fibers.<sup>59,74,75</sup> The foreign body responses after implanting optical devices with various shapes and materials await further examination.

### Recent biological findings at neural electrode-tissue interface

The research on brain tissue and electronic interface using the advanced imaging modalities can be categorized in two major directions. One direction is to characterize and understand the foreign body responses in order to improve the integration and biocompatibility of neural electrodes. The other direction is focused on investigating the cellular mechanisms of electrophysiology recording and stimulation for better decoding and encoding brain activities. Here, we will summarize discoveries from *in vivo* imaging modalities in both directions in recent years.

#### Studies of neurons and neuron-electrode interaction

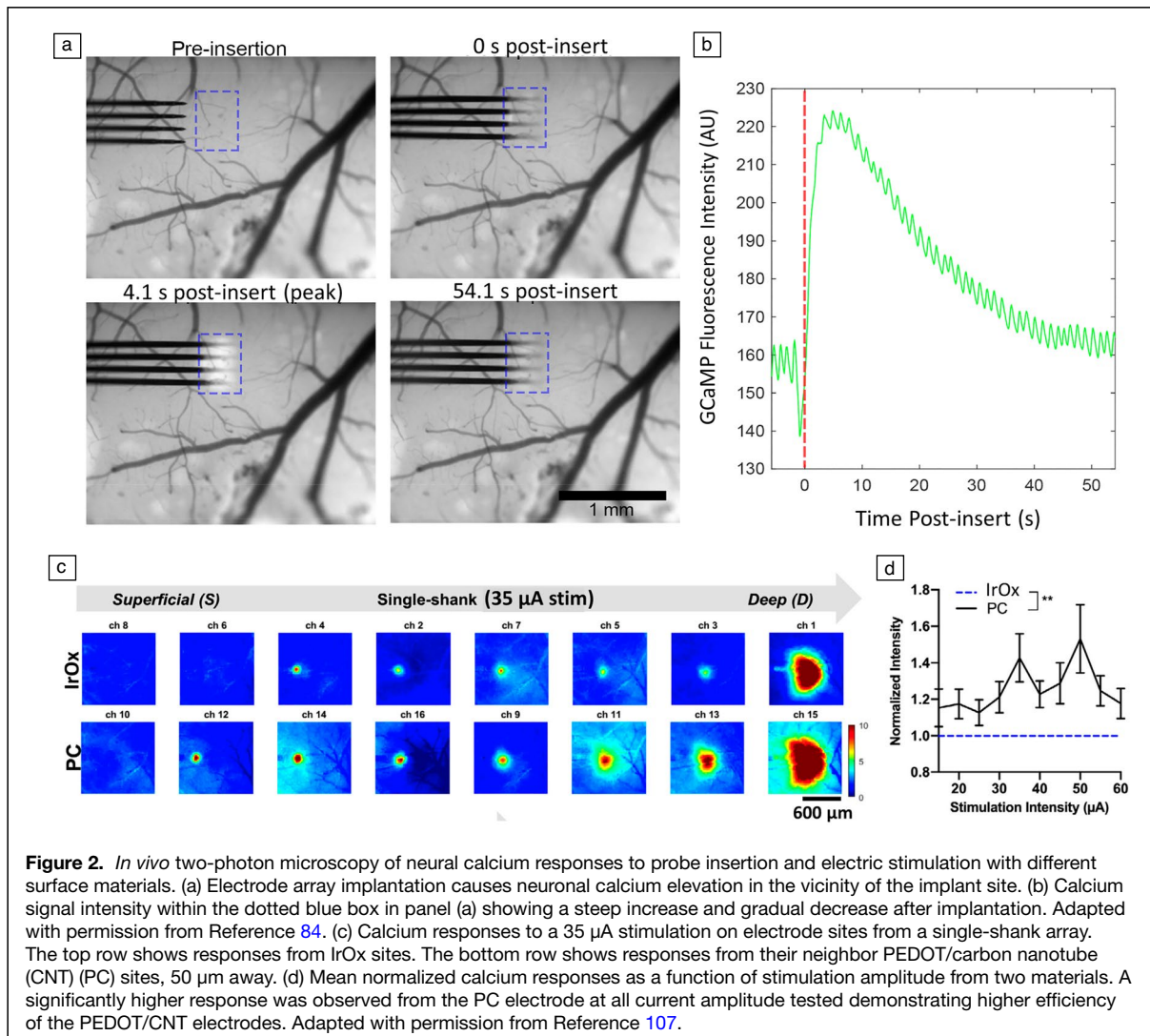
All brain functions, from locomotion, sensing to emotion, learning, and memory, are carried out by neuronal activities. It is estimated that an electrode can detect neuronal action potential signals within a cylinder of 140  $\mu\text{m}$  radius, which contains ~1000 neurons in layer 2/3 of rat cortex.<sup>76–78</sup> Yet in practice, only a few neurons can be reliably identified through electrical recording on each electrode site. This large discrepancy is hypothesized to be due to neural damage by the implanted electrode, or presence of silent neurons or signal amplitude being too small.<sup>78</sup> Electrophysiology recording alone cannot pinpoint these mechanisms because the recordable neuron for an electrode is not only dependent on the distance between the electrode and neuron soma, but also related to the anatomical structures. For example, action potentials from layer 5 pyramidal neurons can be recorded up to 400  $\mu\text{m}$  from the soma along the apical dendrite, but not detectable at 100  $\mu\text{m}$  in the opposite direction.<sup>79</sup> Combining *in vivo* imaging of neural activity and electrophysiology recording has the potential to better uncover the ground truth of extracellular recording. Simultaneous neural calcium imaging and electrophysiology recording have been done with surface ECoG arrays and intracortical microelectrodes.<sup>27,70</sup> Yet, there has not been a conclusive study correlating electrophysiological recording with all recordable neural population activity imaging. With continuous technology advancement in fast, volumetric *in vivo* calcium/voltage imaging, and fabrication of transparent, flexible, and low impedance microelectrode array, this problem is hopefully to be resolved in the near future.

The inserted electrode directly ruptures cell membranes and blood vessels, leading to neuronal death near the implanted device as soon as 1 h postimplantation.<sup>80</sup> The neuronal density drop was observed most dramatically in the first two weeks.<sup>81</sup> After two weeks, the neural degeneration marker was found mostly in neural processes rather than the cell body, and was increasing over time.<sup>80</sup> In addition to neural degeneration, neural activity and excitability could change after electrode implantation.<sup>82</sup> These studies are limited to discrete timepoints due to the postmortem nature of histology method.

*In vivo* multiphoton imaging of neural calcium activity provided an important method to study neuronal health and activity after device implantation in real time, which can be correlated with electrophysiology recording/stimulation.<sup>83</sup> Calcium imaging has been extensively used in neuroscience as calcium influx is associated with most neural depolarization electrical activity.<sup>19</sup> During implantation of microelectrodes in mice cortex, both neuron soma and neurites exhibit abnormally prolonged high calcium levels.<sup>84</sup> Specifically, the neural calcium activity was observed to peak in several seconds

postinsert within 150  $\mu\text{m}$ , then goes down and stabilizes within a minute<sup>84</sup> (Figure 2a–b). After 6 min, the calcium level in neural somas subsided to baseline, while the neurites in layer 1 showed sustained high calcium over 27 min.<sup>84</sup> This calcium elevation is thought to result from the mechanical distortion of neurons and neurites, potentially through mechanoporation,<sup>85</sup> opening of voltage-gated calcium channels triggered by mechanically sensitive sodium channels,<sup>86</sup> or intracellular calcium release.<sup>87</sup> From 1 to 3 h postinsertion, spherical protrusions were observed in the cortical layer 1, suggesting damage to the neurites.<sup>84,88</sup> Additionally, the visually evoked calcium activity around the electrode declined gradually and became unresponsive after two weeks of implantation.<sup>88</sup> In a longer-term study, dendritic arbors of fluorescently labeled layer 5 pyramidal neurons near a multicontact electrode shank were tracked in Thy1-YFP transgenic mice using two-photon microscopy (TPM), where persistent dendritic atrophy was observed for three months.<sup>89</sup>

Electrical stimulation has been widely used in neuroscience research to dissect neural circuitries, and in clinical



treatment of neurological diseases and sensory restorations.<sup>6,90–94</sup> However, what happens between the electrical stimulation and behavior outcomes remains largely unknown. In addition, continuous stimulation can lead to neural reorganization and damage.<sup>95,96</sup> There are emerging studies utilizing simultaneous *in vivo* imaging and electrical stimulation to study the cellular mechanism of electrical stimulation. Early electrophysiology and modeling works suggest that increasing stimulation current leads to increasing radius of neural activation,<sup>97,98</sup> but Histed et al. revealed sparsely distributed neural activation even at low currents using *in vivo* two-photon imaging around the inserted metal wire electrode in layer 2/3.<sup>99</sup> It is explained that distant neurons are activated via neural fibers passing by the electrode tip. In contrast, *ex vivo* studies indicated a laterally confined activation field of cortical microstimulation mainly through transsynaptic activation.<sup>100,101</sup> Using two-photon calcium imaging and iridium microelectrodes on silicon probes inserted into layer 2/3 of mouse cortex, the Kozai group has published a series of works looking at the effects of stimulation parameters and patterns on the spatial and temporal dynamics of neural activity.<sup>102–105</sup> Although these studies began to systematically characterize the neuronal response to microstimulation paradigms, the imaging is only limited to superficial brain layers. By combining transparent and flexible microelectrode array with microprism implantation, Yang et al. expanded the imaging depth and volume, and illustrated the depth dependent neuronal responses of stimulation amplitudes and frequencies across all cortical layers in awake mice.<sup>70</sup>

Microstimulation with high spatial resolution requires advanced electrode materials with high charge injection capacity and stability. As new electrode materials are developed, characterization of the stimulation performance is necessary. Although evaluation of stimulating materials has been conventionally done via *in vitro* and *in vivo* electrochemical tests, electrophysiology and histology, *in vivo* imaging can offer much higher temporal and spatial resolution. To compare newly developed poly(3,4-ethylenedioxythiophene) (PEDOT)/carbon nanotubes (CNTs) (PC) electrode coating to clinically applied iridium oxide (IrOx), Zheng et al. coated silicon probes with PC and IrOx on electrode sites in alternation and evaluated the neuronal calcium activation upon electrical stimulation in head-fixed behaving GCaMP mice for up to 12 weeks.<sup>106,107</sup> Surprisingly, PC electrodes activated a larger and brighter GCaMP response than IrOx (Figure 2c–d) at the same current amplitude, showing higher stimulation efficiency from the PC electrodes.<sup>107</sup> Abnormal ictal cortical responses or cortical spreading depression were observed through the imaging using stimulation parameters commonly considered safe in intracortical stimulation, which could otherwise be overlooked in conventional characterization setup. These studies demonstrate the potential and need to evaluate the efficiency and safety of different electrode materials using real-time imaging.

### Imaging glial responses to implants

As the resident inflammatory cells in the brain, microglia respond rapidly to neural electrode implantation and can initiate cascades of inflammatory responses. In immunohistochemistry studies, activated microglia are found in the vicinity of an implanted electrode, usually surrounded by a dense layer of astrocytes.<sup>108,109</sup> Microglia and astrocytes together form the “glial scar” around the electrode, which is believed detrimental to the signal transduction between the electrode and the neural tissue.<sup>110</sup> Microglial morphology is highly associated with their functional status. In the homeostatic state, microglia have ramified processes protruding almost evenly to all directions. When the brain is damaged, microglia transform to a phagocytic state featured with enlarged cell bodies and shortened processes. Advances in two-photon imaging and transgenic mice that express fluorescent proteins in microglia reveal that in resting state, microglial processes dynamically survey around while the soma stay immobile.<sup>111</sup> These moving processes will make intimate but transient contact with neuronal synapses.<sup>112</sup> This surveillance of microglial processes is dependent on K<sup>+</sup> channel.<sup>113</sup> Once the brain is damaged or injured, surrounding microglia respond rapidly by sending processes toward the injury within several minutes, then depending on the degree of damage, they could become motile and migrate to the injury in several hours, phagocytose cell debris and proliferate in the following days, and remain residing at the injury site for months.<sup>42,72,114,115</sup> The directional response of microglial processes is potentially regulated by ATP release from damaged tissue through G-protein coupled purinergic P2Y receptors.<sup>116</sup> Anesthesia can influence microglial surveillance and activation.<sup>117</sup> Hence, it is important to take careful consideration of the effect of anesthesia while doing live imaging. When possible, imaging in awake animals is recommended for unbiased microglial analysis.

The role of microglia in neuronal health is complex. On one hand, absence of microglia after brain injury leads to much more severe neuronal loss, showing the critical role of microglia in neuroprotection.<sup>118</sup> On the other hand, activated microglia can secrete cytotoxic factors that result in excessive neural degeneration.<sup>119</sup> Modulating the extent of microglia activation to the appropriate level could be the key to improving neuron survival after electrode implantation.<sup>120</sup> Coating of neural electrodes with biomimetic protein or antifouling zwitterionic polymer have been shown to effectively reduce inflammatory responses in postmortem histology studies.<sup>121–123</sup> Recently, using two-photon imaging, the dynamic interactions between the microglia processes and implant surface with and without coatings have been investigated (Figure 3a–b).<sup>47,124</sup> It was revealed that a neuronal adhesion molecule L1 coating inhibited the microglia coverage on the surface of neural probes (Figure 3a).<sup>47</sup> Zwitterionic coating also significantly decreases the microglial coverage, and the mechanism is by suppressing the spreading of microglial end-feet, but not reducing the number (Figure 3b).<sup>124</sup> Anti-inflammatory drugs, such as melatonin

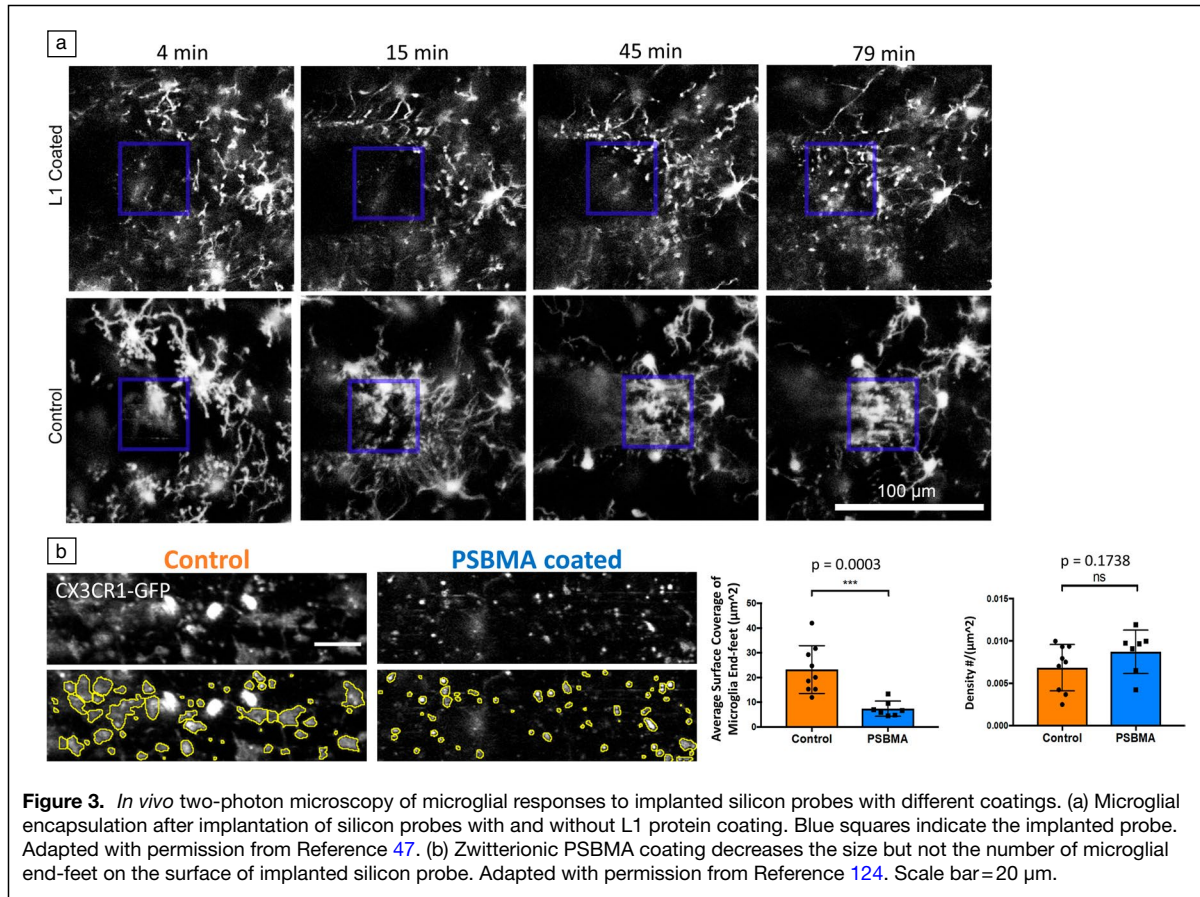


**Figure 3.** *In vivo* two-photon microscopy of microglial responses to implanted silicon probes with different coatings. (a) Microglial encapsulation after implantation of silicon probes with and without L1 protein coating. Blue squares indicate the implanted probe. Adapted with permission from Reference 47. (b) Zwitterionic PSBMA coating decreases the size but not the number of microglial end-feet on the surface of implanted silicon probe. Adapted with permission from Reference 124. Scale bar = 20  $\mu\text{m}$ .

and dexamethasone, have also been shown to attenuate microglial responses and improve electrophysiology recordings.<sup>125–127</sup>

Besides microglia, other types of glial cells in the brain are important for maintaining brain health, including astrocytes, oligodendrocytes, and pericytes. Astrocytes have thin, branchy processes extensively contacting neural synapses and blood vessels.<sup>128</sup> Cumulative evidence indicates that astrocyte processes sense synaptic activity and regulate blood vessel diameters accordingly.<sup>129–131</sup> The perivascular processes of astrocytes also play a critical role in water homeostasis and blood–brain barrier permeability.<sup>132,133</sup> Astrocytes do not produce action potentials like neurons, but they exhibit spontaneous and neural activity correlated intracellular  $\text{Ca}^{2+}$  increases.<sup>134,135</sup> In pathological conditions, activated microglia induce a subtype of reactive astrocytes—termed as A1 astrocytes—by releasing cytokines  $\text{Il-1}\alpha$ ,  $\text{TNF}$ , and  $\text{C1q}$ .<sup>136</sup> A1 astrocytes lose most of the normal neuro-supportive functions and become neurotoxic.<sup>136</sup> The astrocyte response to microelectrode implantation has been characterized using *in vivo* two-photon imaging, showing that astroglia scar develops within the first two weeks and remains stable from week 2 to week 10 postimplantation (Figure 4).<sup>49,137</sup> Two-photon *in vivo* calcium imaging in both neuron and astrocytes reveals that astrocytes start to show calcium response to electrical stimulation at longer pulse width and higher current intensity

than neurons.<sup>138</sup> Moreover, the astrocyte activity is induced by noradrenergic and glutamatergic signaling from neurons.<sup>138</sup>

Oligodendrocytes generate myelin sheaths along axons in the central nervous system (CNS) that can increase the action potential propagation.<sup>139</sup> The myelin sheath development is regulated by neural activity through calcium influx in oligodendrocytes.<sup>140</sup> In addition to myelination, oligodendrocytes also provide neurotrophic and metabolic support to neurons.<sup>141,142</sup> Ablation of oligodendrocytes has been shown to cause neurodegeneration and excessive inflammation.<sup>143,144</sup> Pharmaceutical oligodendrocytes depletion impairs electrophysiology recording quality.<sup>145</sup> A four-week long two-photon imaging study characterized the oligodendrocyte soma deformation and myelinosome formation around implanted silicon electrodes, showing a progressive myelination degeneration (Figure 5a–b).<sup>146</sup>

Oligodendrocyte precursor cells (OPCs) or  $\text{NG2}^+$  cells, the major proliferating cells in the adult CNS, continuously differentiate into myelinating oligodendrocytes in healthy tissue.<sup>147</sup> OPCs play an important role in remyelination, as they can proliferate and differentiate into oligodendrocytes and astrocytes after demyelination.<sup>148–150</sup> *In vivo* two-photon imaging illustrates that OPCs have motile filopodia surveying around, which is similar to microglial processes, but without bulbous endings and move more slowly ( $0.3 \pm$

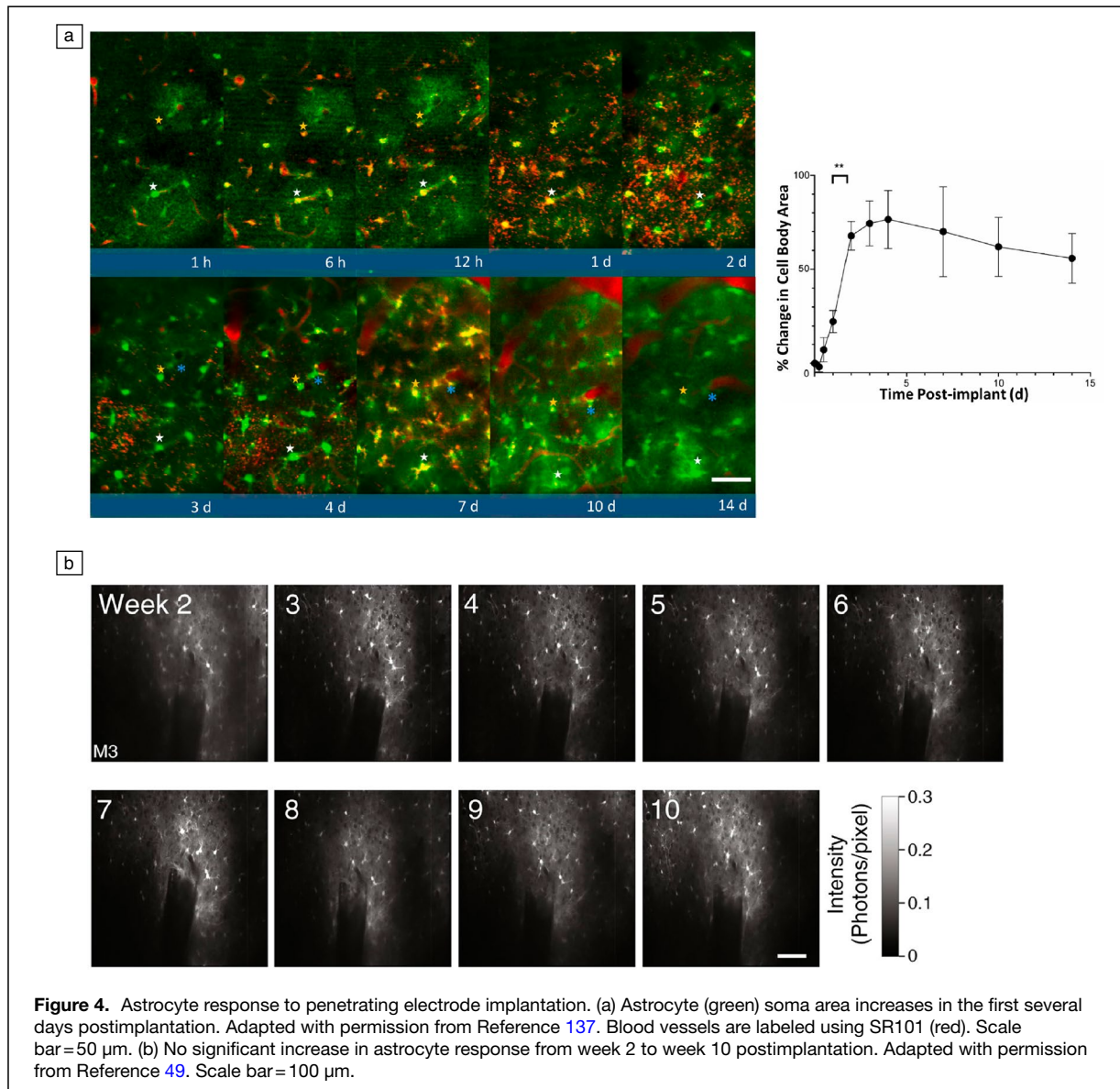


**Figure 4.** Astrocyte response to penetrating electrode implantation. (a) Astrocyte (green) soma area increases in the first several days postimplantation. Adapted with permission from Reference 137. Blood vessels are labeled using SR101 (red). Scale bar = 50  $\mu\text{m}$ . (b) No significant increase in astrocyte response from week 2 to week 10 postimplantation. Adapted with permission from Reference 49. Scale bar = 100  $\mu\text{m}$ .

0.01  $\mu\text{m min}^{-1}$  of OPCs<sup>151</sup> versus  $1.47 \pm 0.1 \mu\text{m min}^{-1}$  of microglia<sup>111</sup>). In addition, most OPCs continuously change their soma locations and processes orientation except for perivascular cells,<sup>151</sup> whereas microglia largely maintain their territory over time. After electrode insertion, OPCs also extend processes toward the implant, but at later time (>12 h) compared to microglia (within several minutes) (Figure 5c–d).<sup>152</sup>

#### Implantation-induced vascular changes

Neural tissue is highly vascularized. Implanting electronic devices inevitably disrupts the vascular network and damage the BBB. The BBB regulates substance exchanges between the peripheral circulation system and the CNS. Vascular endothelial cells together with astrocytes, pericytes, neurons, and the extracellular matrix, form a “neurovascular unit” that is essential for regulating blood flow and BBB

permeability.<sup>153</sup> Vascular damages caused by neural electrodes implantation not only disrupt nutrient and metabolic supply, but also leak the cells and molecules that are cytotoxic to brain tissues.<sup>154</sup> For example, erythrocyte/hemoglobin entry increases iron levels in the brain, which leads to oxidative stress, excitotoxicity, and neuronal injury.<sup>154–157</sup> Cumulative evidence suggests that a higher level of BBB damage is correlated with increased foreign body responses and worse recording performance.<sup>158–160</sup> Two-photon microscopy has the capability to illustrate blood vessel anatomical structures at high resolution and to measure blood flow with injected intravascular fluorescence dyes.<sup>161,162</sup> Localized bleeding as a result of neural probe insertion has been characterized using two-photon microscopy as early as 2009, while shrinkage of capillary and decrease in perfusion at the vicinity of implants have lately been documented.<sup>162</sup> Using OIS-BOLD under wide field microscopy, decreases in blood oxygenation



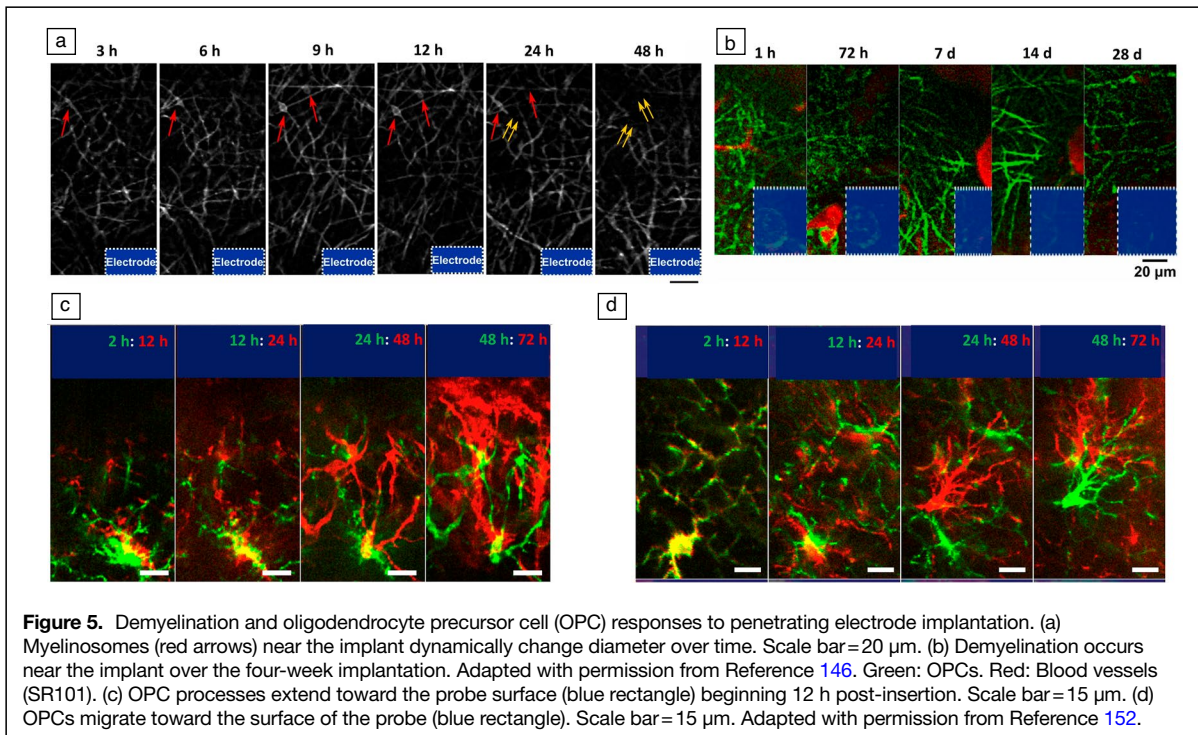


**Figure 5.** Demyelination and oligodendrocyte precursor cell (OPC) responses to penetrating electrode implantation. (a) Myelinosomes (red arrows) near the implant dynamically change diameter over time. Scale bar = 20  $\mu\text{m}$ . (b) Demyelination occurs near the implant over the four-week implantation. Adapted with permission from Reference 146. Green: OPCs. Red: Blood vessels (SR101). (c) OPC processes extend toward the probe surface (blue rectangle) beginning 12 h post-insertion. Scale bar = 15  $\mu\text{m}$ . (d) OPCs migrate toward the surface of the probe (blue rectangle). Scale bar = 15  $\mu\text{m}$ . Adapted with permission from Reference 152.

were observed around the implanted electrode on day 2 and returned to normal levels by day 7.<sup>88</sup> Decreases in blood perfusion could contribute to decreased neural activity in the injured tissue area. With chronic two-photon microscopy, it has been shown that angiogenesis and vascular remodeling are most pronounced in the first two weeks after intracortical implantation of flexible electrodes, coincident with a rapid improvement of electrophysiology recording performance.<sup>45</sup> Chronic two-photon imaging of both microglia and blood vessels reveals persistent microglia aggregations around ablated capillaries, suggesting that BBB breakage even in a single microvessel could lead to long-term inflammation.<sup>72</sup>

### Characterizing meningeal response

The meninges are a thin structure embedding the brain, consisting of three layers in general—dura, arachnoid, and pia matter. Cerebrospinal fluid (CSF) is filled in the subarachnoid space between dura and pia. Recently a fourth layer membrane was uncovered that divides the subarachnoid space into two compartments.<sup>163</sup> There are abundant immune cells residing the meninges, including macrophages and dendritic cells (DCs). Macrophages are numerous in dura and pia and usually respond the quickest to inflammatory stimuli.<sup>164</sup> Although DCs are fewer in number, they are antigen-presenting cells that can stimulate and recruit T cells.<sup>165</sup> The recent discovery of lymphatic vessels in the meninges further highlights the importance of meninges in the immune system.<sup>166,167</sup> The meningeal fibrous encapsulations of neural implants have been well documented in postmortem histology studies for both brain surface arrays and intracortical

implants.<sup>41,168,169</sup> Lymphangiogenesis of meningeal lymphatic vessels and increased CSF influx are more recently reported after implantation of brain surface EEG electrodes.<sup>170</sup> Implanting neural probes into the brain without connection to the meninges has been shown to significantly reduce the glial scar formation compared to trans-meninges unanchored implants, suggesting that part of the glial encapsulation originated from meninges.<sup>171</sup> *In vivo* two-photon microscopy has been used to evaluate meningeal inflammatory responses and meningeal collagen remodeling around implanted silicon probes.<sup>48</sup> The collagen fiber is visualized by second-harmonic generation signal. It is shown that the meningeal inflammatory cell migration along electrodes is most robust during the first day and attenuate by two days post-implantation, while the collagen continues to grow over the next month.<sup>48</sup> Meninges is a potentially powerful target region that can relieve fibrous encapsulation of chronic implants. Our understanding of meningeal responses are still preliminary and remain to be elucidated with more chronic *in vivo* imaging studies.

### Current limitations and future directions

Optical methods for *in vivo* imaging of neural electrode arrays have been vastly progressing in recent years. Direct two-photon imaging of silicon probes inserted at 30–45 degrees in a cranial window has been a popular setup that greatly improved our understanding of dynamic properties of different types of cells in response to electrode implantation. Although it is a facile model, the optically accessible depth is limited to layer 2/3 of cortex and decreases over chronic implantation. Introducing optic fibers, GRIN lenses, or microprisms could help us

gain greater imaging depth. While there are emerging studies on combining optical devices with electrode arrays, most of them are at the stage of proof-of-concept demonstration. Several areas can be further improved for broad applications: (1) The flexible, transparent microelectrodes are more compatible with optical imaging modalities than the commercial silicon probes. However, almost all transparent and flexible arrays are fabricated in individual academic labs. The product quality could vary from batch to batch, and lab to lab. Standardization and commercialization of such flexible and transparent microelectrodes would encourage more usage and accelerate studies in this field. (2) Implanting optical devices generate foreign body responses, which could be a confounding factor for understanding the cellular dynamics at the brain–electronic interface. Multiple timepoints or *in vivo* characterizations of tissue responses to optical devices are needed to validate the methods. Furthermore, it will be beneficial to develop methods to improve the biocompatibility for optical devices, such as antifouling coating, anti-inflammatory coating, etc. (3) Insertion of the optical devices can inevitably cause bleeding that impedes imaging in the first several weeks. To be able to acquire information during that recovery period, technological advancements are necessary. For example, to have a removable cranial window that allows inserting electrodes after the tissue reaction subsides. (4) Flexible electrode arrays for concurrent optical imaging and for the next generation of brain–machine interface are rapidly developing recently. Flexible electrodes have often shown reduced foreign body responses compared to conventional rigid electrodes. Yet, flexible electrodes are usually more difficult to handle and less durable than rigid electrode material wise, and lack quantitative long-term biocompatibility studies. Therefore, flexible electrode devices need to be further studied and optimized in terms of biocompatibility and durability before broad applications. With the continuous technological improvement in *in vivo* fluorescent imaging for neural interfacing electronics, we expect to gather more knowledge on the cellular and subcellular mechanisms related to electrophysiological recording and stimulation, which would greatly help to determine the best electrode material and design in the coming future.

### Conflict of interest

On behalf of all authors, the corresponding author states that there is no conflict of interest.

### Open access

This article is licensed under a Creative Commons Attribution 4.0 International License, which permits use, sharing, adaptation, distribution and reproduction in any medium or format, as long as you give appropriate credit to the original author(s) and the source, provide a link to the Creative Commons license, and indicate if changes were made. The images or other third party material in this article are included in the article's Creative Commons license, unless indicated otherwise in a credit line to the material. If material is not included

in the article's Creative Commons license and your intended use is not permitted by statutory regulation or exceeds the permitted use, you will need to obtain permission directly from the copyright holder. To view a copy of this license, visit <http://creativecommons.org/licenses/by/4.0/>.

### References

1. E. Bizzi, *Exp. Brain Res.* **6**, 69 (1968)
2. H. Asanuma, S. Stoney Jr., C. Abzug, *J. Neurophysiol.* **31**, 670 (1968)
3. S. Miodinovic, S. Somayajula, S. Chitnis, J.L. Vitek, *JAMA Neurol.* **70**, 163 (2013)
4. W.H. Dobelle, *ASAIO J.* **46**, 3 (2000)
5. A.B. Schwartz, X.T. Cui, D.J. Weber, D.W. Moran, *Neuron* **52**, 205 (2006)
6. G.A. Tabot, J.F. Dammann, J.A. Berg, F.V. Tenore, J.L. Boback, R.J. Vogelstein, S.J. Bensmaia, *Proc. Natl. Acad. Sci. U.S.A.* **110**, 18279 (2013)
7. T.D. Kozai, A.S. Jaquins-Gerstl, A.L. Vazquez, A.C. Michael, X.T. Cui, *ACS Chem. Neurosci.* **6**, 48 (2015)
8. A.J. Woolley, H.A. Desai, K.J. Otto, *J. Neural Eng.* **10**, 026007 (2013)
9. J.V. Cramer, B. Gesierich, S. Roth, M. Dichgans, M. Düring, A. Liesz, *Neuroimage* **199**, 570 (2019)
10. Z. Li, Q. Zhang, S.-W. Chou, Z. Newman, R. Turcotte, R. Natan, Q. Dai, E.Y. Isacoff, N. Ji, *Sci. Adv.* **6**, 3870 (2020)
11. R. Shi, C. Jin, H. Xie, Y. Zhang, X. Li, Q. Dai, L. Kong, *Biomed. Opt. Express* **10**, 6625 (2019)
12. M.A. Neil, R. Juškaitis, T. Wilson, *Opt. Lett.* **22**, 1905 (1997)
13. U. Dirnagl, A. Villringer, K.M. Einhügel, *J. Microsc.* **165**, 147 (1992)
14. W. Yu, B. Guo, H. Zhang, J. Zhou, X. Yu, L. Zhu, D. Xue, W. Liu, X. Sun, J. Qian, *Sci. Bull.* **64**, 410 (2019)
15. F. Wang, F. Ren, Z. Ma, L. Qu, R. Gourgues, C. Xu, A. Baghdasaryan, J. Li, I.E. Zadeh, J.W. Los, *Nat. Nanotechnol.* **17**, 653 (2022)
16. F. Xia, M. Gevers, A. Fognini, A.T. Mok, B. Li, N. Akbari, I.E. Zadeh, J. Qin-Dregely, C. Xu, *ACS Photonics* **8**, 2800 (2021)
17. D. Kobat, N.G. Horton, C. Xu, *J. Biomed. Opt.* **16**, 106014 (2011)
18. D. Kobat, M.E. Durst, N. Nishimura, A.W. Wong, C.B. Schaffer, C. Xu, *Opt. Express* **17**, 13354 (2009)
19. C. Stosiek, O. Garaschuk, K. Holthoff, A. Konnerth, *Proc. Natl. Acad. Sci. U.S.A.* **100**, 7319 (2003)
20. A. Cheng, J.T. Gonçalves, P. Golshani, K. Arisaka, C. Portera-Cailliau, *Nat. Methods* **8**, 139 (2011)
21. J.N. Stirman, I.T. Smith, M.W. Kudenov, S.L. Smith, *Nat. Biotechnol.* **34**, 857 (2016)
22. N.J. Sofroniew, D. Flickinger, J. King, K. Svoboda, *eLife* **5**, e14472 (2016)
23. W. Zong, R. Wu, M. Li, Y. Hu, Y. Li, J. Li, H. Rong, H. Wu, Y. Xu, Y. Lu, *Nat. Methods* **14**, 713 (2017)
24. E. Castagnola, X.S. Zheng, X.T. Cui, "Flexible and Soft Materials and Devices for Neural Interface," in *Handbook of Neuroengineering*, ed. by N.V. Thakor (Springer, Singapore, 2023), pp. 79–139
25. Z. Fekete, A. Pongrácz, *Sens. Actuators B Chem.* **243**, 1214 (2017)
26. P. Kshirsagar, S. Dickreuter, M. Mierzejewski, C.J. Burkhardt, T. Chassé, M. Fleischer, P.D. Jones, *Adv. Mater. Technol.* **4**, 1800318 (2019)
27. Y. Lu, X. Liu, R. Hattori, C. Ren, X. Zhang, T. Komiyama, D. Kuzum, *Adv. Funct. Mater.* **28**, 1800002 (2018)
28. A. Zátanyi, M. Madarász, Á. Szabó, T. Lőrincz, R. Hodován, B. Rózsa, Z. Fekete, *J. Neural Eng.* **17**, 016062 (2020)
29. W. Lee, D. Kim, N. Matsuhisa, M. Nagase, M. Sekino, G.G. Malliaras, T. Yokota, T. Someya, *Proc. Natl. Acad. Sci. U.S.A.* **114**, 10554 (2017)
30. C.F. Guo, T. Sun, Q. Liu, Z. Suo, Z. Ren, *Nat. Commun.* **5**, 3121 (2014)
31. Y. Qiang, P. Artoni, K.J. Seo, S. Culaclii, V. Hogan, X. Zhao, Y. Zhong, X. Han, P.-M. Wang, Y.-K. Lo, *Sci. Adv.* **4**, eaat0626 (2018)
32. J. Zhang, X. Liu, W. Xu, W. Luo, M. Li, F. Chu, L. Xu, A. Cao, J. Guan, S. Tang, *Nano Lett.* **18**, 2903 (2018)
33. N. Driscoll, R.E. Rosch, B.B. Murphy, A. Ashourvan, R. Vishnubhotla, O.O. Dickens, A.C. Johnson, K.A. Davis, B. Litt, D.S. Bassett, *Commun. Biol.* **4**, 136 (2021)
34. I. Adawi, *Phys. Rev.* **134**, A788 (1964)
35. W.L. Shew, T. Bellay, D. Pleniz, *J. Neurosci. Methods* **192**, 75 (2010)
36. Y.U. Cho, J.Y. Lee, U.J. Jeong, S.H. Park, S.L. Lim, K.Y. Kim, J.W. Jang, J.H. Park, H.W. Kim, H. Shin, *Adv. Funct. Mater.* **32**, 2105568 (2022)
37. J. Riera, T. Ogawa, R. Hatanaka, T. Goto, A. Sumiyoshi, H.E. Kadji, S. Nakauchi, R. Kawashima, *J. Biophotonics* **3**(3), 147 (2010)
38. A.D. Degenhart, J. Eles, R. Dum, J.L. Mischel, I. Smalianchuk, B. Endler, R.C. Ashmore, E.C. Tyler-Kabara, N.G. Hatsopoulos, W. Wang, *J. Neural Eng.* **13**, 046019 (2016)
39. C. Henle, M. Raab, J.G. Cordeiro, S. Doostkam, A. Schulze-Bonhage, T. Stieglitz, J. Rickert, *Biomed. Microdevices* **13**, 59 (2011)
40. F.Z. Fedor, M. Madarász, A. Zátanyi, Á. Szabó, T. Lőrincz, V. Danda, L. Spurgin, C. Manz, B. Rózsa, Z. Fekete, *Adv. Mater. Technol.* **7**, 2100942 (2022)

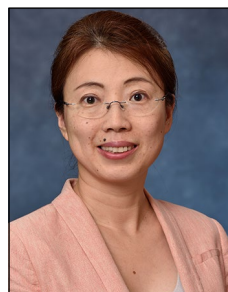
41. A.A. Schendel, M.W. Nonte, C. Vokoun, T.J. Richner, S.K. Brodnick, F. Atry, S. Frye, P. Bostrom, R. Pashaie, S. Thongpang, *J. Neural Eng.* **11**, 046011 (2014)
42. T.D.Y. Kozai, A.L. Vazquez, C.L. Weaver, S.-G. Kim, X.T. Cui, *J. Neural Eng.* **9**, 066001 (2012)
43. T.D. Kozai, J.R. Eles, A.L. Vazquez, X.T. Cui, *J. Neurosci. Methods* **258**, 46 (2016)
44. L. Luan, X. Wei, Z. Zhao, J.J. Siegel, O. Potnis, C.A. Tuppen, S. Lin, S. Kazmi, R.A. Fowler, S. Holloway, *Sci. Adv.* **3**, e1601966 (2017)
45. F. He, Y. Sun, Y. Jin, R. Yin, H. Zhu, H. Rathore, C. Xie, L. Luan, *Biomaterials* **291**, 121905 (2022)
46. X. Liu, C. Ren, Y. Lu, Y. Liu, J.-H. Kim, S. Leutgeb, T. Komiyama, D. Kuzum, *Nat. Neurosci.* **24**, 886 (2021)
47. J.R. Eles, A.L. Vazquez, N.R. Snyder, C. Lagenaur, M.C. Murphy, T.D. Kozai, X.T. Cui, *Biomaterials* **113**, 279 (2017)
48. J. Eles, A. Vazquez, T. Kozai, X. Cui, *Biomaterials* **195**, 111 (2019)
49. K. Mols, S. Musa, B. Nuttin, L. Lagae, V. Bonin, *Sci. Rep.* **7**(1), 15642 (2017)
50. H. Lütcke, M. Murayama, T. Hahn, D.J. Margolis, S. Astori, S. Meyer, W. Göbel, Y. Yang, W. Tang, S. Kügler, *Front. Neural Circuits* **4**, 9 (2010)
51. S.T. Parker, P. Domachuk, J. Amsden, J. Bressner, J.A. Lewis, D.L. Kaplan, F.G. Omenetto, *Adv. Mater.* **21**, 2411 (2009)
52. R. Nazempour, Q. Zhang, R. Fu, X. Sheng, *Materials* (Basel) **11**, 1283 (2018)
53. B.A. Flusberg, E.D. Cocker, W. Piyawattanametha, J.C. Jung, E.L. Cheung, M.J. Schnitzer, *Nat. Methods* **2**, 941 (2005)
54. M. Murayama, E. Pérez-Garci, T. Nevian, T. Bock, W. Senn, M.E. Larkum, *Nature* **457**, 1137 (2009)
55. W. Göbel, J.N. Kerr, A. Nimmerjahn, F. Helmchen, *Opt. Lett.* **29**, 2521 (2004)
56. F. Pisanello, G. Mandelbaum, M. Pisanello, I.A. Oldenburg, L. Sileo, J.E. Markowitz, R.E. Peterson, A. Della Patria, T.M. Haynes, M.S. Emara, *Nat. Neurosci.* **20**, 1180 (2017)
57. F. Pisano, M. Pisanello, S.J. Lee, J. Lee, E. Maglie, A. Balena, L. Sileo, B. Spagnolo, M. Bianco, M. Hyun, *Nat. Methods* **16**, 1185 (2019)
58. R. Nazempour, B. Zhang, Z. Ye, L. Yin, X. Lv, X. Sheng, *Adv. Fiber Mater.* **2021**, 1 (2021)
59. Y. Zhou, C. Gu, J. Liang, B. Zhang, H. Yang, Z. Zhou, M. Li, L. Sun, T.H. Tao, X. Wei, *Microsyst. Nanoeng.* **8**, 118 (2022)
60. A. Canales, X. Jia, U.P. Friep, R.A. Koppes, C.M. Tringides, J. Selvidge, C. Lu, C. Hou, L. Wei, Y. Fink, *Nat. Biotechnol.* **33**, 277 (2015)
61. G. Cui, S.B. Jun, X. Jin, M.D. Pham, S.S. Vogel, D.M. Lovinger, R.M. Costa, *Nature* **494**, 238 (2013)
62. A.R. Rouse, A. Kano, J.A. Udovich, S.M. Kroto, A.F. Gmitro, *Appl. Opt.* **43**, 5763 (2004)
63. J.C. Jung, A.D. Mehta, E. Aksay, R. Stepnoski, M.J. Schnitzer, *J. Neurophysiol.* **92**, 3121 (2004)
64. M.J. Levene, D.A. Dombeck, K.A. Kasischke, R.P. Molloy, W.W. Webb, *J. Neurophysiol.* **91**, 1908 (2004)
65. R.P. Barretto, T.H. Ko, J.C. Jung, T.J. Wang, G. Capps, A.C. Waters, Y. Ziv, A. Attardo, L. Recht, M.J. Schnitzer, *Nat. Med.* **17**, 223 (2011)
66. L.F. Cobar, A. Kashef, K. Bose, A. Tashiro, *Sci. Rep.* **12**, 736 (2022)
67. M.L. Andermann, N.B. Gilfoy, G.J. Goldey, R.N. Sachdev, M. Wölfel, D.A. McCormick, R.C. Reid, M.J. Levene, *Neuron* **80**, 900 (2013)
68. M. Murayama, E. Pérez-Garci, H.-R. Luscher, M.E. Larkum, *J. Neurophysiol.* **98**, 1791 (2007)
69. P. Kim, E. Chung, H. Yamashita, K.E. Hung, A. Mizoguchi, R. Kucherlapati, D. Fukumura, R.K. Jain, S.H. Yun, *Nat. Methods* **7**, 303 (2010)
70. Q. Yang, B. Wu, E. Castagnola, M.Y. Pwint, A.L. Vazquez, X.T. Cui, *bioRxiv* (2022). <https://doi.org/10.1101/2022.07.08.499369>
71. L. Beckmann, X. Zhang, N.A. Nadkarni, Z. Cai, A. Batra, D.P. Sullivan, W.A. Muller, C. Sun, R. Kuranov, H.F. Zhang, *Biomed. Opt. Express* **10**, 5235 (2019)
72. Q. Yang, A.L. Vazquez, X.T. Cui, *Biomaterials* **276**, 121060 (2021)
73. Y.-T. Kim, R.W. Hitchcock, M.J. Bridge, P.A. Tresco, *Biomaterials* **25**, 2229 (2004)
74. L. Wang, C. Zhong, D. Ke, F. Ye, J. Tu, L. Wang, Y. Lu, *Adv. Opt. Mater.* **6**, 1800427 (2018)
75. S. Park, H. Yuk, R. Zhao, Y.S. Yim, E.W. Woldegebriel, J. Kang, A. Canales, Y. Fink, G.B. Choi, X. Zhao, P. Anikeeva, *Nat. Commun.* **12**(1), 3435 (2021)
76. D.A. Henze, Z. Borhegyi, J. Csicsvari, A. Mamiya, K.D. Harris, G. Buzsáki, *J. Neurophysiol.* **84**, 390 (2000)
77. C. Holmgren, T. Harkany, B. Svennerfors, Y. Zilberter, *J. Physiol.* **551**, 139 (2003)
78. G. Buzsáki, *Nat. Neurosci.* **7**, 446 (2004)
79. G.R. Buzsáki, A. Kandel, *J. Neurophysiol.* **79**, 1587 (1998)
80. G.C. McConnell, H.D. Rees, A.I. Levey, C.-A. Gutekunst, R.E. Gross, R.V. Bellamkonda, *J. Neural Eng.* **6**, 056003 (2009)
81. M. Ravikumar, S. Sunil, J. Black, D.S. Barkauskas, A.Y. Haung, R.H. Miller, S.M. Selkirk, J.R. Capadona, *Biomaterials* **35**, 8049 (2014)
82. J.W. Salatino, B.M. Winter, M.H. Drazin, E.K. Purcell, *J. Neurophysiol.* **118**, 194 (2017)
83. H. Dana, T.-W. Chen, A. Hu, B.C. Shields, C. Guo, L.L. Looger, D.S. Kim, K. Svoboda, *PLoS ONE* **9**, e108697 (2014)
84. J.R. Eles, A.L. Vazquez, T.D. Kozai, X.T. Cui, *Biomaterials* **174**, 79 (2018)
85. P.R. Williams, B.-N. Marincu, C.D. Sorbara, C.F. Mahler, A.-M. Schumacher, O. Griesbeck, M. Kerschensteiner, T. Misgeld, *Nat. Commun.* **5**(1), 5683 (2014)
86. J.A. Wolf, P.K. Stys, T. Lusardi, D. Meaney, D.H. Smith, *J. Neurosci.* **21**, 1923 (2001)
87. J.A. Staal, T.C. Dickson, R. Gasperini, Y. Liu, L. Foa, J.C. Vickers, *J. Neurochem.* **112**, 1147 (2010)
88. N.J. Michelson, A.L. Vazquez, J.R. Eles, J.W. Salatino, E.K. Purcell, J.J. Williams, X.T. Cui, T.D. Kozai, *J. Neural Eng.* **15**, 033001 (2018)
89. C.G. Welle, Y.-R. Gao, M. Ye, A. Lozzi, A. Boretsky, E. Abliz, D.X. Hammer, *Biomaterials* **238**, 119831 (2020)
90. S.N. Flesher, J.L. Collinger, S.T. Foldes, J.M. Weiss, J.E. Downey, E.C. Tyler-Kabara, S.J. Bensmaia, A.B. Schwartz, M.L. Boninger, R.A. Gaunt, *Sci. Transl. Med.* **8**, 361ra141 (2016)
91. C.L. Hughes, S.N. Flesher, J.M. Weiss, M. Boninger, J.L. Collinger, R.A. Gaunt, *eLife* **10**, e65128 (2021)
92. J. Siegfried, B. Lippitz, *Neurosurgery* **35**, 1126 (1994)
93. L. D'Alatri, G. Paludetti, M.F. Contarino, S. Galla, M.R. Marchese, A.R. Bentivoglio, *J. Voice* **22**, 365 (2008)
94. P. Limousin, P. Krack, P. Pollak, A. Benazzouz, C. Ardouin, D. Hoffmann, A.-L. Benabid, *N. Engl. J. Med.* **339**, 1105 (1998)
95. D. McCreery, V. Píkov, P.R. Troyk, *J. Neural Eng.* **7**, 036005 (2010)
96. M.M. Chakravarty, C. Hamani, A. Martinez-Canabal, J. Ellegood, C. Laliberté, J.N. Nobrega, T. Sankar, A.M. Lozano, P.W. Frankland, J.P. Lerch, *Neuroimage* **125**, 422 (2016)
97. E. Tehovnik, A. Talias, F. Sultan, W. Slocum, N. Logothetis, *J. Neurophysiol.* **96**, 512 (2006)
98. S. Stoney Jr., W. Thompson, H. Asanuma, *J. Neurophysiol.* **31**, 659 (1968)
99. M.H. Histed, V. Bonin, R.C. Reid, *Neuron* **63**, 508 (2009)
100. A.T. Hussin, J.A. Boychuk, A.R. Brown, Q.J. Pittman, G.C. Teskey, *Brain Stimul.* **8**, 742 (2015)
101. Y. Tanaka, T. Nomoto, T. Shiki, Y. Sakata, Y. Shimada, Y. Hayashida, T. Yagi, *J. Neural Eng.* **16**, 036007 (2019)
102. N.J. Michelson, J.R. Eles, A.L. Vazquez, K.A. Ludwig, T.D. Kozai, *J. Neurosci. Res.* **97**, 620 (2019)
103. J.R. Eles, K.C. Stieger, T.D. Kozai, *J. Neural Eng.* **18**, 015001 (2021)
104. K.C. Stieger, J.R. Eles, K.A. Ludwig, T.D. Kozai, *J. Neurosci. Res.* **98**, 2072 (2020)
105. J.R. Eles, T.D. Kozai, *Biomaterials* **234**, 119767 (2020)
106. X.S. Zheng, Q. Yang, A. Vazquez, X.T. Cui, *iScience* **25**, 104539 (2022)
107. X.S. Zheng, Q. Yang, A. Vazquez, X.T. Cui, *Adv. Nanobiomed. Res.* **1**(7), 2000092 (2021)
108. V.S. Polikov, P.A. Tresco, W.M. Reichert, *J. Neurosci. Methods* **148**(1), 1 (2005)
109. D. Szarowski, M. Andersen, S. Retterer, A. Spence, M. Isaacson, H.G. Craighead, J. Turner, W. Shain, *Brain Res.* **983**, 23 (2003)
110. D. McCreery, S. Cogan, S. Kane, V. Píkov, *J. Neural Eng.* **13**, 036012 (2016)
111. A. Nimmerjahn, F. Kirchhoff, F. Helmchen, *Science* **308**, 1314 (2005)
112. H. Wake, A.J. Moorhouse, S. Jinno, S. Kohsaka, J. Nabekura, *J. Neurosci.* **29**, 3974 (2009)
113. C. Madry, V. Kyrgaryri, I.L. Arancibia-Cárcamo, R. Jolivet, S. Kohsaka, R.M. Bryan, D. Attwell, *Neuron* **97**, 299 (2018)
114. S.J. Ahn, J. Anrather, N. Nishimura, C.B. Schaffer, *Stroke* **49**, 1719 (2018)
115. T.M. Rotterman, F.J. Alvarez, *Sci. Rep.* **10**, 8648 (2020)
116. D. Davalos, J. Grutzendler, G. Yang, J.V. Kim, Y. Zuo, S. Jung, D.R. Littman, M.L. Dustin, W.-B. Gan, *Nat. Neurosci.* **8**, 752 (2005)
117. W. Sun, K. Suzuki, D. Toptunov, S. Stoyanov, M. Yuzaki, L. Khiroug, A. Dityatev, *Front. Neurosci.* **13**, 421 (2019)
118. J. Neumann, M. Gunzer, H.O. Gutzzeit, O. Ullrich, K.G. Reymann, K. Dinkel, *FASEB J.* **20**, 714 (2006)
119. R.B. Banati, J. Gehrmann, P. Schubert, G.W. Kreutzberg, *Glia* **7**, 111 (1993)
120. M. Schwartz, *J. Cereb. Blood Flow Metab.* **23**, 385 (2003)
121. A. Golabchi, K.M. Woepffel, X. Li, C.F. Lagenaur, X.T. Cui, *Biosens. Bioelectron.* **155**, 112096 (2020)
122. A. Golabchi, B. Wu, B. Cao, C.J. Bettinger, X.T. Cui, *Biomaterials* **225**, 119519 (2019)
123. E. Azemi, C.F. Lagenaur, X.T. Cui, *Biomaterials* **32**, 681 (2011)
124. Q. Yang, B. Wu, J.R. Eles, A.L. Vazquez, T.D. Kozai, X.T. Cui, *Adv. Biosyst.* **4**, 190287 (2020)
125. D.D. Krahe, K.M. Woepffel, Q. Yang, N. Kushwah, X.T. Cui, *Antioxidants* (Basel) **11**, 1628 (2022)
126. A. Golabchi, B. Wu, X. Li, D.L. Carlisle, T.D. Kozai, R.M. Friedlander, X.T. Cui, *Biomaterials* **180**, 225 (2018)
127. Y. Zhong, R.V. Bellamkonda, *Brain Res.* **1148**, 15 (2007)
128. K. Kacem, P. Lacombe, J. Seylaz, G. Bonvento, *Glia* **23**, 1 (1998)
129. C. Iadecola, M. Nedergaard, *Nat. Neurosci.* **10**, 1369 (2007)
130. M.V. Sofroniew, H.V. Vinters, *Acta Neuropathol.* **119**, 7 (2010)
131. R.C. Koehler, R.J. Roman, D.R. Harder, *Trends Neurosci.* **32**, 160 (2009)
132. M. Simard, G. Arcuino, T. Takano, Q.S. Liu, M. Nedergaard, *J. Neurosci.* **23**, 9254 (2003)
133. M. Simard, M. Nedergaard, *Neuroscience* **129**, 877 (2004)

134. A.H. Cornell-Bell, S.M. Finkbeiner, M.S. Cooper, S.J. Smith, *Science* **247**, 470 (1990)
135. H. Hirase, L. Qian, P. Barthó, G. Buzsáki, *PLoS Biol.* **2**, e96 (2004)
136. S.A. Liddelow, K.A. Guttenplan, L.E. Clarke, F.C. Bennett, C.J. Bohlen, L. Schirmer, M.L. Bennett, A.E. Münch, W.-S. Chung, T.C. Peterson, *Nature* **541**, 481 (2017)
137. S.P. Savva, F. Li, S. Lam, S.M. Wellman, K.C. Stieger, K. Chen, J.R. Eles, T.D. Kozai, *Biomaterials* **289**, 121784 (2022)
138. Z. Ma, L. Wei, X. Du, S. Hou, F. Chen, Q. Jiao, A. Liu, S. Liu, J. Wang, H. Shen, *J. Neural Eng.* **18**, 046096 (2021)
139. G.S. Tomassy, D.R. Berger, H.-H. Chen, N. Kasthuri, K.J. Hayworth, A. Vercelli, H.S. Seung, J.W. Lichtman, P. Arlotta, *Science* **344**, 319 (2014)
140. A.M. Krasnow, M.C. Ford, L.E. Valdivia, S.W. Wilson, D. Attwell, *Nat. Neurosci.* **21**, 24 (2018)
141. A.S. Saab, I.D. Tzvetavona, A. Trevisiol, S. Baltan, P. Dibaj, K. Kusch, W. Möbius, B. Goetze, H.M. Jahn, W. Huang, *Neuron* **91**, 119 (2016)
142. A.I. Amaral, T.W. Meisingset, M.R. Kotter, U. Sonnewald, *Front. Endocrinol.* **4**, 54 (2013)
143. M. Nakano, Y. Tamura, M. Yamato, S. Kume, A. Eguchi, K. Takata, Y. Watanabe, Y. Kataoka, *Sci. Rep.* **7**, 42041 (2017)
144. I. Griffiths, M. Klugmann, T. Anderson, D. Yool, C. Thomson, M.H. Schwab, A. Schneider, F. Zimmermann, M. McCulloch, N. Nadon, *Science* **280**, 1610 (1998)
145. S.M. Wellman, K. Guzman, K.C. Stieger, L.E. Brink, S. Sridhar, M.T. Dubaniewicz, L. Li, F. Cambi, T.D. Kozai, *Biomaterials* **239**, 119842 (2020)
146. K. Chen, S.M. Wellman, Y. Yaxiaer, J.R. Eles, T.D. Kozai, *Biomaterials* **268**, 120526 (2021)
147. M.R. Dawson, A. Polito, J.M. Levine, R. Reynolds, *Mol. Cell. Neurosci.* **24**, 476 (2003)
148. R.B. Tripathi, L.E. Rivers, K.M. Young, F. Jamen, W.D. Richardson, *J. Neurosci.* **30**, 16383 (2010)
149. A.R. Hackett, D.-H. Lee, A. Dawood, M. Rodriguez, L. Funk, P. Tsoufias, J.K. Lee, *Neurobiol. Dis.* **89**, 10 (2016)
150. J.M. Levine, R. Reynolds, *Exp. Neurol.* **160**, 333 (1999)
151. E.G. Hughes, S.H. Kang, M. Fukaya, D.E. Bergles, *Nat. Neurosci.* **16**, 668 (2013)
152. S.M. Wellman, T.D. Kozai, *Biomaterials* **164**, 121 (2018)
153. B.T. Hawkins, T.P. Davis, *Pharmacol. Rev.* **57**, 173 (2005)
154. C. Bennett, F. Mohammed, A. Álvarez-Ciara, M.A. Nguyen, W.D. Dietrich, S.M. Rajguru, W.J. Streit, A. Prasad, *Biomaterials* **188**, 144 (2019)
155. L. Goldstein, Z.P. Teng, E. Zeserson, M. Patel, R.F. Regan, *J. Neurosci. Res.* **73**, 113 (2003)
156. J. Wang, *Prog. Neurobiol.* **92**, 463 (2010)
157. C.C. Winterbourn, *Toxicol. Lett.* **82**, 969 (1995)
158. T. Saxena, L. Karumbaiah, E.A. Gaupp, R. Patkar, K. Patil, M. Betancur, G.B. Stanley, R.V. Bellamkonda, *Biomaterials* **34**, 4703 (2013)
159. N.F. Nolte, M.B. Christensen, P.D. Crane, J.L. Skousen, P.A. Tresco, *Biomaterials* **53**, 753 (2015)
160. L. Grand, L. Wittner, S. Herwik, E. Göthelid, P. Ruther, S. Oscarsson, H. Neves, B. Dombovári, R. Csercsa, G. Karmos, *J. Neurosci. Methods* **189**, 216 (2010)
161. A.Y. Shih, J.D. Driscoll, P.J. Drew, N. Nishimura, C.B. Schaffer, D. Kleinfeld, *J. Cereb. Blood Flow Metab.* **32**, 1277 (2012)
162. T.D.Y. Kozai, T.C. Marzullo, F. Hooi, N.B. Langhals, A. Majewska, E. Brown, D.R. Kipke, *J. Neural Eng.* **7**, 046011 (2010)
163. K. Møllgård, F.R. Beinlich, P. Kusk, L.M. Miyakoshi, C. Delle, V. Plá, N.L. Hauglund, T. Esmail, M.K. Rasmussen, R.S. Gomolka, *Science* **379**, 84 (2023)
164. Y. Lavin, A. Mortha, A. Rahman, M. Merad, *Nat. Rev. Immunol.* **15**, 731 (2015)
165. H.R. Chinnery, M.J. Ruitenberg, P.G. McMenamin, *J. Neuropathol. Exp. Neurol.* **69**(9), 896 (2010)
166. A. Louveau, I. Smirnov, T.J. Keyes, J.D. Eccles, S.J. Rouhani, J.D. Peske, N.C. Derecki, D. Castle, J.W. Mandell, K.S. Lee, *Nature* **523**, 337 (2015)
167. J.A. Coles, P.J. Stewart-Hutchinson, E. Myburgh, J.M. Brewer, *Methods* **127**, 53 (2017)
168. X. Cui, J. Wiler, M. Dzaman, R.A. Altschuler, D.C. Martin, *Biomaterials* **24**, 777 (2003)
169. P.A. Cody, J.R. Eles, C.F. Lagenaur, T.D. Kozai, X.T. Cui, *Biomaterials* **161**, 117 (2018)
170. N.L. Hauglund, P. Kusk, B.R. Kornum, M. Nedergaard, *J. Neurosci.* **40**, 2371 (2020)
171. N.T. Markwardt, J. Stokol, R.L. Rennaker II., *J. Neurosci. Methods* **214**, 119 (2013) □

**Publisher's note** Springer Nature remains neutral with regard to jurisdictional claims in published maps and institutional affiliations.



**Qianru Yang** is a doctoral candidate at the University of Pittsburgh. She earned her BS degree in biology from the University of Science and Technology of China in 2015. Her research has been focused on *in vivo* two-photon fluorescent microscopy of the neural electrode-tissue interface, including antifouling coating material, acute and chronic inflammatory responses to neural implants, application of microprism implantation in neural tissue engineering, and investigating cellular mechanisms of electrophysiology recording and stimulation. Yang can be reached by email at qiy24@pitt.edu.



**X. Tracy Cui** is the William Kepler Whiteford Professor of Bioengineering at the University of Pittsburgh. She earned her PhD degree in macromolecular science and engineering from the University of Michigan. She works in the field of neural engineering with special focuses on the neural electrode-tissue interface, neural tissue engineering, drug delivery, and biosensors. She is a senior member of the National Academy of Inventors, Fellow of the Royal Society of Chemistry, Fellow of the American Institute for Medical and Biological Engineering, and a recipient of the Carnegie Science Emerging Female Scientist Award. Cui can be reached by email at xic11@pitt.edu.